www.elsevier.com/locate/jmbbm

Age-related Changes in dynamic moduli of ovine vitreous

Jourdan Colter, Alex Williams, Patrick Moran, Brittany Coats

PII: S1751-6161(14)00288-4
DOI: http://dx.doi.org/10.1016/j.jmbbm.2014.09.004
Reference: JMBBM1262

To appear in: *Journal of the Mechanical Behavior of Biomedical Materials*

Received date: 2 May 2014
Revised date: 30 August 2014
Accepted date:
2 September 2014

Cite this article as: Jourdan Colter, Alex Williams, Patrick Moran, Brittany Coats, Age-related Changes in dynamic moduli of ovine vitreous, *Journal of the Mechanical Behavior of Biomedical Materials,* http://dx.doi.org/10.1016/j.jmbbm.2014.09.004

Age-related Changes in Dynamic Moduli of Ovine Vitreous

Jourdan Colter[1], Alex Williams[1], Patrick Moran[2], and Brittany Coats[2]

[1] Department of Bioengineering, University of Utah
James LeVoy Sorenson Molecular Biotechnology Building (SMBB)
36 S. Wasatch Drive, Rm. 3100
Salt Lake City, UT 84112, USA
Phone: (801) 581-8528

[2] Department of Mechanical Engineering, University of Utah
Merrill Engineering Building
50 S. Central Campus Dr., Room 2110
Salt Lake City, UT 84112, USA
Phone: (801) 581-6441

Corresponding Author:

Brittany Coats

Merrill Engineering Building
50 S. Central Campus Dr., Room 2110
Salt Lake City, UT 84112, USA
Phone: (801) 585-0586
E-mail: brittany.coats@utah.edu

Keywords: ocular mechanics, pediatric, rheometry, dynamic material analysis, spectrum interconversion

ABSTRACT

Multiple rheological studies have characterized the dynamic material properties of adult vitreous, but no studies have investigated vitreous properties in the immature eye. In this study, premature, infant and adult ovine vitreous specimens were tested in shear to identify differences in dynamic moduli with age. Significant inertial artifact and rapid degradation of the vitreous *ex vivo* hindered the ability to accurately collect dynamic data through standard oscillation protocols. Therefore, dynamic moduli in this study were calculated by converting relaxation spectrum data to the retardation spectrum, resulting in the calculation of the storage (G') and loss (G") moduli from the first few milliseconds of creep testing when tissue degradation and inertia is minimal. The technique was validated against two synthetic materials that span the viscoelastic spectrum. G' and G" of the primarily viscous synthetic material (polystyrene, $\tan\delta = 0.61$) and G' of the primarily elastic material (agar, $\tan\delta = 0.06$) were not significantly different than those calculated from dynamic oscillatory testing ($p<0.05$). G" of agar was overestimated (4-39%) with the interconversion technique due to creep ringing. Ovine vitreous was primarily viscous ($\tan\delta = 1.31$), so this technique was used to evaluate changes in dynamic moduli with age. G' and G" for adult vitreous was 2-4 times and 1.5-2 times lower, respectively, than infant vitreous, corresponding to the structural breakdown of the vitreous with age. The dynamic moduli of premature vitreous was lower than infant and adult, likely due to premature development of the vitreal structure. These data suggest that significant differences exist between the viscoelastic

response of infant and adult vitreous, and computational models of the pediatric eye will require appropriate age and rate material properties of vitreous.

1. INTRODUCTION

In the U.S., there are an estimated 160,000 to 280,000 eye injuries every year in children (<15 years of age) that are serious enough to cause in-patient hospitalization (Abbott and Shah, 2013). Finite element (FE) analysis is a valuable computational tool that provides insight into the responses of an eye during trauma. Many FE models exist for investigating ocular injury and pathologies of the adult eye (Amini, et al., 2011;Djilas, et al., 2011;Girard, et al., 2011;Kasi, et al., 2011;Nguyen and Boyce, 2011;Opie, et al., 2010;Power, et al., 2002;Rossi, et al., 2011;Roy and Dupps, 2011;Sigal, 2011;Uchio, et al., 2004;Uchio, et al., 1999;Weaver, et al., 2011;Yang, et al., 2009), but only two FE models exist for pediatric ocular research (Hans, et al., 2009;Rangarajan, et al., 2009). Both of these models utilize adult material properties, many of which were tested at quasistatic rates, and are likely to be a misrepresentation of the pediatric ocular mechanical response to trauma. Studies have qualitatively noted differences in mechanical properties between infant and adult ocular tissues, but these studies lack quantifiable data necessary to construct a FE model of the pediatric eye (Berman and Michaelson, 1964;Bishop, et al., 2004;Denlinger, et al., 1980;Los, et al., 2003;Sebag, 1987;Walton, et al., 2002).

The vitreous body is a gelatinous and collagenous substance that fills the inner posterior cavity of the eye. While vitreous is comprised of mostly water (~99% by weight), the unique extracellular matrix made up of collagen and hyaluronan significantly contributes to the viscoelastic nature of the vitreous (Filas, et al., 2014;Nickerson, C.S., et al., 2008;Sebag and

Balazs, 1989;Sharif-Kashani, et al., 2011). As the eye ages, the collagen networks begin to break down and pockets of liquid form (Sebag, 1987). This results in obvious structural and mechanical differences between pediatric and adult vitreous. Because the vitreous makes up a large percentage of the mass of the eye, its material properties will be necessary to characterize and accurately develop an FE model of the pediatric eye.

The objective of this study is to quantify differences between the viscoelastic response of mature and immature vitreous in order to develop more accurate computational models of the pediatric eye. We hypothesize that the immature vitreous will have a higher loss and storage modulus due to the more intact collagen network compared to the adult. To test this hypothesis, we measured the dynamic material properties on premature (128-136 days gestation), infant (~150 days gestation) and adult ovine vitreous. There are no official studies comparing the development of the sheep eye at birth to those of a newborn, however, sheep eyes in general have the same macromolecular organization compared to human eyes (Noulas, et al., 2004;Ponsioen, et al., 2010). Additionally, qualitative assessments of the age-dependent collagen distributions in the sheep eye currently being collected in our lab are similar to those reported in humans. Combined, these data suggest the ovine eye may be suitable for investigating age-related changes in vitreous mechanics.

Characterizing the *in vivo* material properties of the vitreous is challenging. Nickerson et al. (2008) used rheometry to test the dynamic properties of adult bovine and porcine vitreous and noted that the vitreous rapidly degrades upon excision. Dynamic shear testing was only representative of the *in vivo* state within the first few minutes of testing. Vitreous was also highly susceptible to low signal-to-noise ratios at low frequencies, resonant effects, slipping at surface loading, and tool inertia effects at frequencies > 1 Hz (Ewoldt and McKinley, 2007;Nickerson

and Kornfield, 2005). Preliminary studies in our lab found a similar degradation of the vitreous with time and significant instrument inertial effects. Instrument inertia was minimized by developing a smaller tool made of more lightweight material, but these changes were only able to extend the dynamic frequency for reliable data up to 0.1 Hz. Computational simulations of pediatric abusive or accidental head trauma will likely require higher frequencies for accurate simulation. Shaking, a form of abusive head trauma, has been reported to result in a cyclic head frequency of 2-3 Hz (Prange, et al., 2003). Accidental trauma will likely experience higher frequencies as head impact is a common characteristic (Case, 2008). Therefore, in order to accurately estimate the eye's response in accidental or abusive head trauma, the dynamic material properties of pediatric vitreous will be required at frequencies greater than 2 Hz.

To achieve reliable data at higher frequencies than 0.1 Hz, we evaluated a technique called interconversion. Interconversion estimates dynamic frequency-dependent moduli from time-dependent creep test data by converting from the retardation spectrum to the relaxation spectrum. The methodology used in this study was developed by J. Honorkamp and J. Weese (1993) and has been used mostly in rheological studies of polymers (Bradshaw and Brinson, 1997;Kaschta and Schwarzl, 1994;Partal, et al., 1999;Ringhofer, et al., 1997;Wasserman, 1995), but it has also been used in the rheological characterization of liver tissue (Liu and Bilston, 2000). In this study, we first validate this technique with two synthetic materials ranging in viscoelasticity, and then use it to quantify differences in the dynamic material response between premature, infant and adult ovine vitreous.

2. METHODS AND MATERIALS

2.1 Synthetic Materials

To validate the interconversion technique, a primarily viscous material (polystyrene-toluene) and primarily elastic material (agarose) were selected. To create the polystyrene-toluene mixture, polystyrene atactic flakes (Polysciences, Inc., Warrington, PA) with a molecular weight of 50,000 Da were dissolved in toluene to a final concentration of approximately 60% by mass. Small volumes ($0.6cm^3$-$2.5cm^3$) of the solution were placed on the rheometer plates and maintained at a temperature of 20° C during testing.

Dry agarose (Sigma-Aldrich, St. Louis, MO) was mixed with deionized water to a concentration of 1% by volume. After thoroughly mixing, the agarose was heated in the microwave until it began to boil. The mixture was stirred a second time and poured into a Petri dish, covered, and immediately cooled in a fridge at 9°C for at least 12 hours to gel completely. Using a 20 mm trephine, agarose samples were delicately removed from the Petri dish and placed on the rheometer parallel plates maintained at 20°C for testing.

2.2 Ovine vitreous

Eyes from premature (n=13), infant (n=11) and adult (n=6) sheep were collected immediately post-mortem from non-ocular related animal studies and stored in phosphate buffered saline (PBS). All testing occurred within 24 hours of death. Previous studies have shown that vitreous mechanical properties do not significantly change within 24 hours post-mortem as long as all surrounding tissues are kept intact (Weber, et al., 1982). On the date of testing, the extraocular tissue (muscle, fat, etc.) was removed using forceps. The optic nerve was transected at the scleral and optic nerve junction to allow direct access to the peripapillary sclera.

The sclera and choroid were dissected up to the corneoscleral junction by accessing the small cavity between the choroid and retina, and bluntly dissecting with forceps. The retina was then carefully peeled away from the vitreous leaving only the vitreous and hyaloid membrane. The entire vitreous and hyaloid membrane was placed onto the parallel rheometer plates and maintained at 37.5°C. A vapor trap filled with 37° water covered the specimen to maintain a humid environment.

2.3 Mechanical Testing

All synthetic and biological specimens were tested in shear using an AR-G2 rheometer (TA Instruments, New Castle, DE) with accompanying Rheology Advantage Instrument Control software. To prevent slipping, commercial cross-hatched parallel plate geometries (TA Instruments, New Castle, DE, Fig. 1A) and in-house custom parallel plate geometries (Fig. 1B) were designed to better grip the samples during testing. The commercial cross-hatched plates were made of steel and consisted of triangular cleats with an overall height of 0.5 mm from the base of the plate. The custom cleats were made of ABS and consisted of square (0.36 mm^2) cleats that were 0.9 mm high. All synthetic material testing was completed using the commercial geometry and vitreous testing was completed with the custom geometry. The addition of cleats to a parallel plate alters the location of the no-slip boundary layer during testing. Therefore, an effective gap height or gap correction factor was required for the custom geometry (Nickerson and Kornfield, 2005). To validate the cleat design and identify the gap correction factors, forced oscillation tests were performed on low viscosity standard Newtonian oil (Cannon Oils, State Collge, PA) and polydimethylsiloxane (PDMS) putty using both smooth plates and the custom plates. Four gap heights were evaluated (500 μm, 1000 μm, 1500 μm and 2000 μm). The calculated gap correction factor was determined to be 325 μm for the commercial geometry and

393 μm for the custom cleat geometry. Using these correction factors resulted in no significant difference in dynamic moduli between the smooth plates and the custom plates (Figure 2).

The linear viscoelastic region (LVR) was established for each material by subjecting preliminary samples (n=3) to a strain sweep over three decades (0.1-100%) at 1 Hz. The two synthetic materials (n=6 for each material) were then subjected to a dynamic frequency sweep (forced oscillation) and a creep test. The order of the frequency and creep test was rotated (i.e. frequency/creep, creep/frequency) from one sample to the next to account for carryover effects due to the dependent testing. Forced oscillation frequencies swept from 0.1 to100 rad/s at 1% strain, which was within in the LVR of both materials. For creep testing, PS and agarose were subjected to a torque of 35 μNm and 15 μNm, respectively, and held for 90 seconds. The stresses resulting from these applied torques were in the LVR.

Due to the rapid degradation of the vitreous, only creep testing was performed on the vitreous by applying 0.25 μNm torque and holding this load for 90 seconds. The stress resulting from this torque was within the LVR of immature and mature vitreous. To approximate the accuracy of our post-processing interconversion technique on vitreous, two pairs of eyes from two infant sheep were extracted. The left eye was used for creep testing. The right eye only experienced forced oscillation testing. Resulting dynamic moduli from both tests were compared.

3. DATA ANALYSIS

3.1 Interconversion

All creep tests were converted post hoc to frequency-dependent data using a previously developed interconversion technique composed of 3 steps as shown in Figure 3A (Elster, et al., 1991;Honerkamp and Weese, 1993). First, time-dependent creep data is fit to an intermediate

material function, $J(t)$, where J_0 and η_0 are the instantaneous compliance and zero shear viscosity, respectively. Compliances, J_k, represent the spectral strengths at each retardation timescale λ_k (Equation 1). Collectively, J_k and λ_k are known as the discrete retardation spectrum, $L_d(\lambda)$ (Fig. 3B). This spectrum is then interconverted to the discrete relaxation spectrum, $H_d(\tau)$, defined by a set of characteristic moduli, G_i, each with timescale, τ_i (Fig. 3C). The relaxation modulus, $G(t)$, is defined using this spectrum and an equilibrium modulus, G_e (Equation 2). The dynamic moduli, $G'(\omega)$ and $G''(\omega)$, are related to the spectra and are calculated by Equations (3) and (4).

$$J(t) = J_0 + \sum_{k=1}^{m} J_k \left[1 - e^{-t/\lambda_k}\right] + \frac{t}{\eta_0} \tag{1}$$

$$G(t) = G_e + \sum_{i=1}^{n} G_i e^{-t/\tau_i} \tag{2}$$

$$G'(\omega) = G_e + \omega \int_0^{\infty} \left[G(t) - G_e\right] \sin(\omega t)\, dt \tag{3}$$

$$G''(\omega) = \omega \int_0^{\infty} \left[G(t) - G_e\right] \cos(\omega t)\, dt \tag{4}$$

The reliable dynamic range of calculated G' and G" is defined by the reliable time range of creep data. The lower limit of the converted frequency data must correspond to the reciprocal of the total time for the creep data. For example, creep tests in this study were run for 90 seconds, so the lower limit of the resulting frequency range was 1/90 Hz. Similarly, the upper limit of the converted frequency data must correspond to the reciprocal of the lowest resolvable value from the creep tests. This value varied depending on the signal-to-noise ratio and the presence and duration of the toe region. The interconversion process was performed sequentially

in *Advanced Polymer Library* software (TA Instruments, New Castle, DE). A more in depth description of interconversion theory has been written by J.D. Ferry (1980).

Creep ringing is a phenomenon that results from the coupling of the sample's elasticity with the rheometer's inertia (Ewoldt and McKinley, 2007), and has an appearance of an under-damped system. Interconversion of data with creep ringing caused error in preliminary studies. In order to minimize this error, an averaging technique was developed using MATLAB (MathWorks, Inc. v. 8.0.0) in which the ringing was damped by averaging the peak-to-valley distances. All the peak and valley data points were selected for averaging with the origin included as a valley. By averaging the peak-to-valley data, the system was effectively critically damped and ringing was minimized.

3.2 Statistics

Statistical analysis was performed using JMP (SAS Institute Inc. v. 11.0.0). For each synthetic material, a paired Student's t-test (α=0.05) was used at each frequency to test for significant differences between G' and G" obtained from forced oscillation tests and those calculated from interconverted creep test data. Material property differences among ovine vitreous at different ages (premature, infant and adult) were analyzed using a one-way ANOVA test for each frequency. A post-hoc Tukey's Honestly Significantly Difference test was used to perform individual age comparisons for both G' and G" at each frequency.

4. RESULTS

4.1 Polystyrene-Toluene & Agarose

The creep test of the predominantly viscous PS solution resulted in little to no creep ringing (Fig. 4). Therefore, the interconversion of this data was completed without averaging any data points. The paired t-tests indicated that only the last two frequencies of G' and last frequency of G" calculated from the creep data were statistically different from G' and G" calculated from oscillation data ($p<0.05$, Fig. 5A-B). The deviations at these higher frequencies were most likely caused by the presence of a slight toe region and some minor noise in the PS creep data for the first ~0.1 seconds.

Agar creep tests resulted in substantial creep ringing for the initial 5 to 7 seconds of the test (Fig. 4). The ringing was minimized by using the averaging technique described in the methods. The subsequent interconverted G′ was not significantly different from that of forced oscillation and resulted in an excellent approximation of G' for the entire interconverted frequency spectrum (Fig. 5C). The interconverted G" accurately predicted G" near the edges of the frequency range evaluated with forced oscillation, but was significantly different between 0.04 – 0.63 Hz ($p<0.05$, Fig. 5D). The maximum error was 38.5% at 0.1Hz. The minimum error was 4% at 1.6Hz.

4.2 Ovine Vitreous

The creep response of the ovine vitreous was dominantly more viscous, but produced small amounts of creep ringing, depending on the animal age (Fig. 6). Vitreous ringing was at a much lower amplitude and frequency than the ringing present in agarose. The ringing was corrected using the same averaging technique that was applied to the agarose. A relatively long

toe region in the creep tests restricted the resolvable upper limit of the interconverted frequency spectrum to 1 Hz.

At low frequencies (0.01-0.03 Hz), the interconverted dynamic moduli were similar to the moduli determined from forced oscillation testing from the left and right eyes of two infant sheep (Fig. 7). As frequency and testing time increased, the dynamic moduli from forced oscillation descreased, indicative of degradation of the specimens. Differences between the means of interconverted and forced oscillation G' increased sequentially 0.9-10.2 Pa for frequencies up to 0.3 Hz. Differences between the means of interconverted and forced oscillation G" increased sequentially 1.6-12.8 Pa for frequencies up to 0.3 Hz. At 0.3 Hz, instrument inertia effects, and potentially slipping, resulted in unstable forced oscillation data and could no longer be trusted. The interconversion technique was able to extend the dynamic range to 1 Hz. The interconversion technique was not able to extend further than this point due to small signal to noise ratios and a toe region at the beginning of the creep data.

Infant vitreous had larger storage and loss moduli at every frequency. Premature and adult vitreous G' were nearly equivalent at frequencies under 0.06 Hz, but then adult G' followed a similar increasing trend as the infant modulus, while premature vitreous was less affected by frequency (Fig. 8A). For the loss modulus, infant, adult and premature vitreous increased with relatively similar trends and had G" values of 170.86 Pa, 121.14 Pa and 98.14 Pa, respectively, at 1 Hz (Fig. 8B). There were no significant differences between the ages due to high variability in the interconverted data. The gap heights for premature, infant and adult vitreous were 2708±658 μm, 3258±879 μm and 4746±947 μm, respectively. A correlation analysis verified that gap height was independent of the calculated dynamic moduli for each age.

5. DISCUSSION

The complex nature of vitreous results in a challenging biological material to characterize dynamically. Within minutes after extraction from the globe, the vitreous begins to release hyaluronan, creating a layer of lubrication at the boundary plates. This significantly alters the material properties of the vitreous from its *in vivo* state, and leads to slipping at high frequencies. Furthermore, weak gel-like substances, such as vitreous, can be significantly affected by instrument inertia at high frequencies. In this study, we overcame these challenges by using spectrum interconversion to calculate frequency data from the first few milliseconds of a creep test. Validation of this technique was performed on synthetic, non-degrading materials. No significant differences in G' and G" at frequencies less than 10 Hz were found when using the technique on the primarily viscous polystyrene-toulene ($\tan \delta = 0.62 \pm 0.10$). An error of 38% existed for frequencies greater than 10 Hz due to minor noise in the initial few data points of the creep compliance curve, highlighting the constraint that the highest frequency of the interconverted data set is dependent on the lowest resolvable value from the creep data. For agar, G' was accurately calculated by the methodology, but estimates of G" were overestimatd in the center of the frequency range (0.4-0.6 Hz). This is not surprising as Schwarzl (1970) theoretically evaluated the calculation of G' and G" from creep compliance data and noted that G' is a fairly easy calculation that will typically result in accurate estimates, but G" is more challenging to compute and may lead to errors in the estimates, especially in underdamped systems (i.e., materials with low $\tan\delta$ values such as agar). The average $\tan \delta$ of the agar mixture was 0.06 ± 0.01 and exhibited substantial creep ringing. We speculated that eliminating the ringing with an averaging technique could significantly reduce the error. This speculation was supported by initial tests using the interconversion technique on creep data with and without

averaging. Without averaging, estimates of G" of agar were up to 4,608% greater than the forced oscillation measurements. Averaging the creep ringing mitigated this error down to 21-40% and there was no significant difference between the interconverted and forced oscillation moduli < 0.4 Hz or between 0.6 Hz and 3 Hz. Similar techniques such as smoothing or filtering of experimental data have been used in previous studies involving spectra conversion (Brabec and Schausberger, 1995;Emri and Tschoegl, 1993;Hansen, 2008;Kaschta and Schwarzl, 1994), but we found our averaging technique performed better than attempts at general smoothing or filtering.

Vitreous is a primarily viscous material (tan δ = 1.31±0.54). The ratio between G' and G" was smaller in the infant (tan δ = 1.12±0.17) and premature (tan δ = 0.94±0.7) vitreous compared to the adult vitreous (tan δ = 1.89±0.33), but overall the creep tests and tan δ of each age were more similar to polystyrene than agar. Therefore, interconversion was assumed to be a valid methodology for obtaining accurate dynamic data. Validating this assumption directly with vitreous was unfeasible due to rapid degradation *ex vivo*. Therefore, to estimate the accuracy of the assumption, data from interconverted creep tests of the left eye of two animals were compared to forced oscillation tests of the right eye from the same two animals. The G' and G" calculated using the interconversion method were only slightly higher than the right eye oscillation tests during the stable frequency range, indicating that the method provides a close approximation of the dynamic values. Of importance, the measured moduli from the forced oscillation tests became unstable after 0.3 Hz due to inertial effects and slipping. The interconversion technique was able to extend the dynamic frequency range up to 1 Hz. Moduli at higher frequencies could not be obtained due to the limitations of using this technique on biological tissues. The relationship between the frequency and time dependent responses are

inverse of one another. This means that the highest frequencies will be obtained from the earliest data points of the creep data set. As with most biological specimens, vitreous exhibited a toe region at the beginning of the creep curve. Only data after this toe region could be used in the interconversion technique, thus higher frequencies above 1 Hz were not resolvable. Future studies might be able decrease the length of the toe regio by increasing the rate of stress application in the creep tests.

Nickerson et al. (2008) and Sharif-Kashani et al. (2011) directly measure the dynamic moduli from adult porcine vitreous up to 10 rad/s (~1.6 Hz) using forced oscillation. Nickerson et al. was able to use forced oscillationbecause the ARES-RFS rheometer used in the study decouples the torque load cell from the instrument and therefore eliminates inertia artifact. It is unclear if Sharif-Kashani et al. evaluated inertial effects, but their reported dynamic moduli are similar to the steady-state dynamic moduli reported by Nickerson et al. after the initial rapid degradation of the specimen. Therefore, the inertial effects may have been minimal. The adult eye is more viscous than the immature eye and is likely less susceptible to inertia artifacts resulting from the coupling of the material's elasticity to the instrument inertia.

Using the interconversion technique to evaluate the age dependence of vitreous, infant and adult properties followed a pattern concurrent with known structural changes in the vitreous with age. The vitreous is composed of a network of collagen fibers filled with hyaluronan. One of the major roles of hyaluronan is to bind to water and saturate the collagen networks. With age, the collagen fibers degrade. Additionally, the hyaluronan expels from the collagen networks and forms pockets of fluid in the vitreous. The breakdown of the collagen decreases the stiffness and structural integrity of the vitreous, as illustrated by the lower storage modulus in the adult ovine eye compared to the infant (Fig. 8A). The expelling of hyaluronan from the networks, and

formation of pockets of fluid in the vitreous, results in an overall decrease in the damping characteristics of the network and reduces the loss modulus (Fig. 8B). These data correspond to the findings of Filas et al. (2014), who enzymatically digested collagen and hyaluronan and found a decrease in the storage moduli for both. The digestion of hyaluronan led to a decrease in tan δ, suggesting a greater decrease to the loss modulus compared to the storage modulus. The digestion of collagen led to an increase in tan δ. The tan δ of the adult vitreous in this study was greater than that of infant, suggesting that the degradation of the collagen is a larger contributing factor to the change in dynamic properties with age.

The premature vitreous yielded dynamic moduli that were lower than both the infant and adult vitreous. This is likely attributed to the fact that the collagen networks of the premature sheep eye are not fully developed. The rate of change in G' and G" with frequency was also much smaller in the premature vitreous compared to the adult and infant. The infant and adult vitreous dynamic moduli increased with similar non-linear patterns with increased frequency. The premature vitreous had a much more gradual increase in dynamic moduli with increasing frequency. This suggests that the hyaluronan may not be fully integrated into the collagen networks in the premature sheep eye.

There was a definite distinction between the mean values of the dynamic moduli with age. However, these differences were not statistically significant due to large standard deviations and relatively small (n=6-13) sample sizes. Some of the variability can be attributed to natural animal-to-animal variability, but additional deviations may have been caused by the sensitivity of the vitreous to handling upon extraction from the globe. Retina was carefully peeled from the vitreous prior to testing. This task may take longer in some eyes compared to others. All eyes were tested within 2 minutes of extraction, but some dissections were faster. The standard

deviations were also notably larger at higher frequencies than lower frequencies. Higher frequencies from the interconverted data correlate to the earliest, or most instantaneous, data of the creep compliance curve. Nickerson et al. (2008) reported larger standard deviations when measuring initial dynamic moduli of adult porcine and bovine vitreous as compared to steady-state dynamic moduli. This attribute may reflect the rate of degradation in the vitreous. Degradation changes are rapid initially and then slow down over time, reaching a steady state. This degradation appears to affect the storage and loss moduli uniformly as the variability for tan δ calculations were 2 orders of magnitude smaller than variability for the dynamic moduli.

Calculating dynamic material moduli of vitreous through the specialized interconversion technique increases the dynamic range and reduces the effects of the rapidly degrading vitreous *ex vivo* and instrument inertia on the accuracy of the measurements. This method was used to quantify the age and rate dependent dynamic moduli of ovine vitreous. Concurrent with age-related changes in microstructural integrity, the infant vitreous had larger G' and G" than adult vitreous, and generally exhibited more elastic characteristics. Premature vitreous was more similar to that of adult vitreous as the development of the collagen network and integration of hyaluronan had not yet formed. Given these structural changes and associated differences in material properties, age-appropriate material data will be required for representing the vitreous in dynamic simulations of ocular trauma in children and adults.

ACKNOWLEDGMENTS

The authors thank Kurt Albertine and the Neonatal Chronic Lung Disease and Development Lab at the University of Utah for donating ovine ocular tissue. Also greatly appreciated is the funding granted by the Knights Templar Eye Foundation.

REFERENCES

Abbott, J. and Shah, P., 2013. The epidemiology and etiology of pediatric ocular trauma. Surv Ophthalmol. 58. 476-485

Amini, R., Barocas, V.H., Kavehpour, H.P. and Hubschman, J.P., 2011. Computational simulation of altitude change-induced intraocular pressure alteration in patients with intravitreal gas bubbles. Ret. 31. 1656-1663

Berman, E.R. and Michaelson, I.C., 1964. The chemical composition of the human vitreous body as related to age and myopia. Exp Eye Res. 3. 9-15

Bishop, P.N., Holmes, D.F., Kadler, K.E., McLeod, D. and Bos, K.J., 2004. Age-related changes on the surface of vitreous collagen fibrils. IOVS. 45. 1041-1046

Brabec, C. and Schausberger, A., 1995. An improved algorithm for calculating relaxation time spectra from material functions of polymers with monodisperse and bimodal molar mass distributions. Rheol Acta. 34. 397-405

Bradshaw, R. and Brinson, L., 1997. A sign control method for fitting and interconverting material functions for linear viscoelastic solids. Mech Time Dep Mat. 1. 85-108

Case, M., 2008. Accidental traumatic head injury in infants and young children. Brain Path. 18. 583-589

Denlinger, J.L., Eisner, G. and Balazs, E.A., 1980. Age-related changes in the vitreus and lens of rhesus monkeys (macaca mulatta). Exp Eye Res. 31. 67-79

Djilas, M., Olès, C., Lorach, H., Bendali, A., Dégardin, J., Dubus, E., Lissorgues-Bazin, G., Rousseau, L., Benosman, R., Ieng, S.H., Joucla, S., Yvert, B., Bergonzo, P., Sahel, J. and Picaud, S., 2011. Three-dimensional electrode arrays for retinal prostheses: Modeling, geometry optimization and experimental validation. J Neur Eng. 8.

Elster, C., Honerkamp, J. and Weese, J., 1991. Using regularization methods for the determination of relaxation and retardation spectra of polymeric liquids. Rheol Acta. 30. 161-174

Emri, I. and Tschoegl, N., 1993. Generating line spectra from experimental responses: I - relaxation modulus and creep compliance. Rheol Acta. 32. 311-321

Ewoldt, R.H. and McKinley, G.H., 2007. Creep ringing in rheometry or how to deal with oft-discarded data in step stress tests. Rheol. Bull. 76.

Ferry, J.D., 1980. Viscoelastic properties of polymers, Wiley and Sons, New York

Filas, B.A., Zhang, Q., Okamoto, R.J., Shui, Y.-B. and Beebe, D.C., 2014. Enzymatic degradation identifies components responsible for the structural properties of the vitreous body. IOVS. 55. 55-63

Girard, M.J.A., Suh, J.K.F., Bottlang, M., Burgoyne, C.F. and Downs, J.C., 2011. Biomechanical changes in the sclera of monkey eyes exposed to chronic iop elevations. IOVS. 52. 5656-5669

Hans, S.A., Bawab, S.Y. and Woodhouse, M.L., 2009. A finite element infant eye model to investigate retinal forces in shaken baby syndrome. Graefes Arch Clin Exp Ophthalmol. 247. 561-571

Hansen, S., 2008. Estimation of the relaxation spectrum from dynamic experiments using bayesian analysis and a new regularization contraint. Rheol Acta. 47. 169-178

Honerkamp, J. and Weese, J., 1993. A nonlinear regularization method for the calculation of relaxation spectra. Rheol Acta. 32. 57-64

Kaschta, J. and Schwarzl, F., 1994. Calculation of discrete retardation spectra from creep data - i. Method. Rheol Acta. 33. 517-529

Kasi, H., Bertsch, A., Guyomard, J.-L., Kolomiets, B., Picaud, S., Pelizzone, M. and Renaud, P., 2011. Simulations to study spatial extent of stimulation and effect of electrode–tissue gap in subretinal implants. Med Eng & Phy. 33. 755-763

Liu, Z. and Bilston, L.E., 2000. On the viscoelastic character of liver tissue: Experiments and modeling of the linear behavior. Biorheol. 37. 191-201

Los, L.I., Worp, R.J.v.d., Luyn, M.J.A.v. and Hooymans, J.M.M., 2003. Age-related liquefaction of the human vitreous body: Lm and tem evaluation of the role of proteoglycans and collagen. IOVS. 44. 2828-2833

Moran, P., 2012. Characterization of the vitreoretinal interface and vitreous in the porcine eye as it changes with age. Mechanical Engineering, University of Utah. Salt Lake City

Nguyen, T.D. and Boyce, B.L., 2011. An inverse finite element method for determining the anisotropic properties of the cornea. Biomech Mod Mechanobio. 10. 323-337

Nickerson, C., Park, J., Kornfield, J. and Karageozian, H., 2008. Rheological properties of the vitreous and the role of hyaluronic acid. J Bimoechanics. 41. 1840-1846

Nickerson, C.S. and Kornfield, J.A., 2005. A “cleat” geometry for suppressing wall slip. J of Rheol. 49. 865-874

Nickerson, C.S., Park, J., Kornfield, J.A. and Karageozian, H., 2008. Rheological properties of the vitreous and the role of hyaluronic acid. J Biomech. 41. 1840-1846

Noulas, A., Skandalis, S., Feretis, E., Theocharis, D. and Karamano, N., 2004. Variations in content and structure of glycosaminoglycans of the vitreous gel from different mammalian species. Biom Chrom. 18. 457-461

Opie, N.L., Burkitt, A.N., Meffin, H. and Grayden, D.B., 2010. Thermal heating of a retinal prosthesis: Thermal model and in-vitro study. Conf Proc IEEE Eng Med Biol Soc. 2010. 1597-1600

Partal, P., Martinez-Boza, F., Conde, b. and Gallegos, C., 1999. Rheological characterization of synthetic binders and unmodified bitumens. Fuel. 78. 1-10

Ponsioen, T., Hooymans, J. and Los, L., 2010. Remodelling of the human vitreous and vitreoretinal interface - a dynamic process. Prog Ret Eye Res. 29. 580-595

Power, E., Duma, S., Stitzel, J., Herring, I., West, R., Bass, C., Crowley, J. and Brozoski, F., 2002. Computer modeling of airbag-induced ocular injury in pilots wearing night vision goggles. Aviat Space Environ Med. 73. 1000-1006

Prange, M., Coats, B., Duhaime, A.C. and Margulies, S., 2003. Anthropomorphic simulations of falls, shakes, and inflicted impacts in infants. J Neurosurg. 99. 143-150

Rangarajan, N., Kamalakkannan, S., Hasija, V., Shams, T., Jenny, C., Serbanescu, I., Ho, J., Rusinek, M. and Levin, A., 2009. Finite element model of ocular injury in abusive head trauma. Journal of AAPOS. 13. 364-369

Ringhofer, M., Brabec, C., Sobezak, R., Mead, D. and Driscoll, J., 1997. Investigation of the linear flow regime of commercial polymers by numerical conversion of mvm creep measurements. Rheologica Acta. 36. 657-666

Rossi, T., Boccassini, B., Esposito, L., Iossa, M., Ruggiero, A., Tamburrelli, C. and Bonora, N., 2011. The pathogenesis of retinal damage in blunt eye trauma: Finite element modeling. IOVS. 52. 3994-4002

Roy, A.S. and Dupps, W.J., 2011. Patient-specific computational modeling of keratoconus progression and differential responses to collagen cross-linking. IOVS. 52. 9174-9187

Schwarzl, F., 1970. On the interconversion between viscoelastic material functions. Pure and Applied Chemistry. 23. 219-234

Sebag, J., 1987. Age-related changes in human vitreous structure. Graefe's Arch Clin Exp Ophthalmol. 225. 89-93

Sebag, J. and Balazs, E.A., 1989. Morphology and ultrastructure of human vitreous fibers. Investigative Ophthalmology & Visual Sciences. 30. 1867-1871

Sharif-Kashani, P., Hubschman, J.-P., Sassoon, D. and Kavehpour, H.P., 2011. Rheology of the vitreous gel: Effects of macromolecule organization on the viscoelastic properties. Journal of Biomechanics. 44. 419-423

Sigal, I.A., 2011. An applet to estimate the iop-induced stress and strain within the optic nerve head. IOVS. 52. 5497-5506

Uchio, E., Kadonosono, K., Matsuoka, Y., Ed and Goto, S., 2004. Simulation of air-bag impact on an eye with transsclerally fixated posterior chamber intraocular lens using finite element analysis. Journal of Cataract & Refractive Surgery. 30. 483-490

Uchio, E., Ohno, S., Kudoh, J., Aoki, K. and Kisielewicz, L.T., 1999. Simulation model of an eyeball based on finite element analysis on a supercomputer. Br J Ophthalmol. 83. 1106-1111

Walton, K.A., Meyer, C.H., Harkrider, C.J., Cox, T.A. and Toth, C.A., 2002. Age-related changes in vitreous mobility as measured by video b scan ultrasound. Experimental Eye Research. 74. 173-180

Wasserman, S., 1995. Calculating the molecular weight distribution form linear viscoelastic response of polymer melts. Journal of Rheology. 39. 601-625

Weaver, A.A., Loftis, K.L., Duma, S.M. and Stitzel, J.D., 2011. Biomechanical modeling of eye trauma for different orbit anthropometries. Journal of Biomechanics. 44. 1296-1303

Weber, H., Landwehr, G., Kilp, H. and Neubauer, H., 1982. The mechanical properties of the vitreous of pig and human donor eyes. Ophthalmic Res. 14. 335-343

Yang, Y.F., Zhang, J., Wang, X.H., Wang, Q., Mei, J. and Zeng, Y.J., 2009. Simulation of corneal tissue mechanical deformation due to laser thermokeratoplasty: A finite element methods study. Australas Phys Eng Sci Med. 32. 220-225

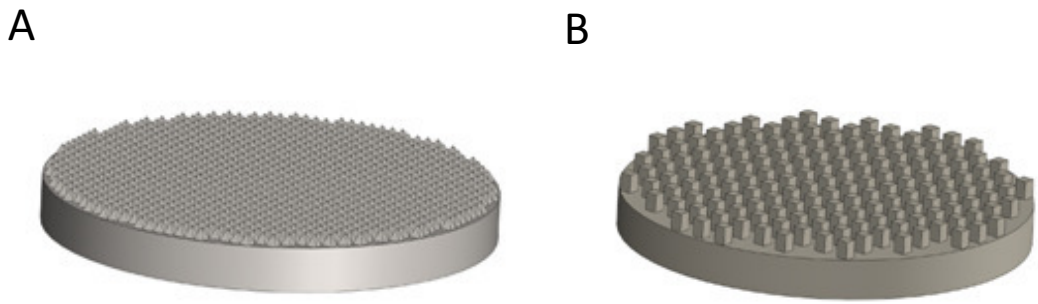

Figure 1: Two plate geometries were used to reduce wall slip between the sample and rheometer. (A) Commercial plate geometry 90^{o} x 0.5mm deep, apex to apex, steel (TA Instruments, New Castle, DE). (B) Custom plate geometry 0.6mm x0.6mm x0.9mm (LxWxH) 13.70mm diameter ABS.

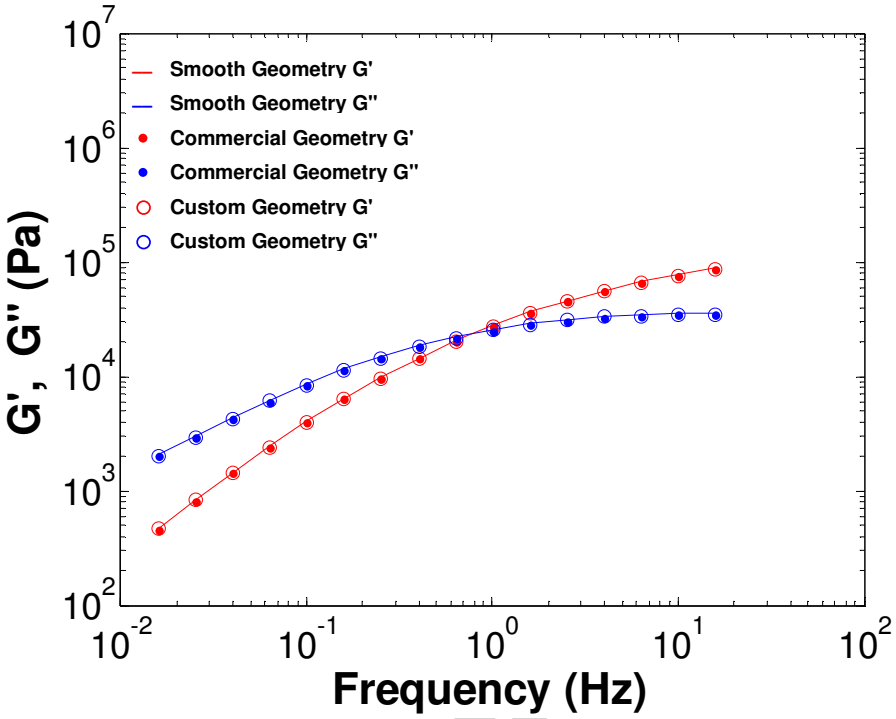

Figure 2: Performing forced oscillations on PDMS with different rheometer plate geometries and associated gap heights validated the cleat design and gap correction factors

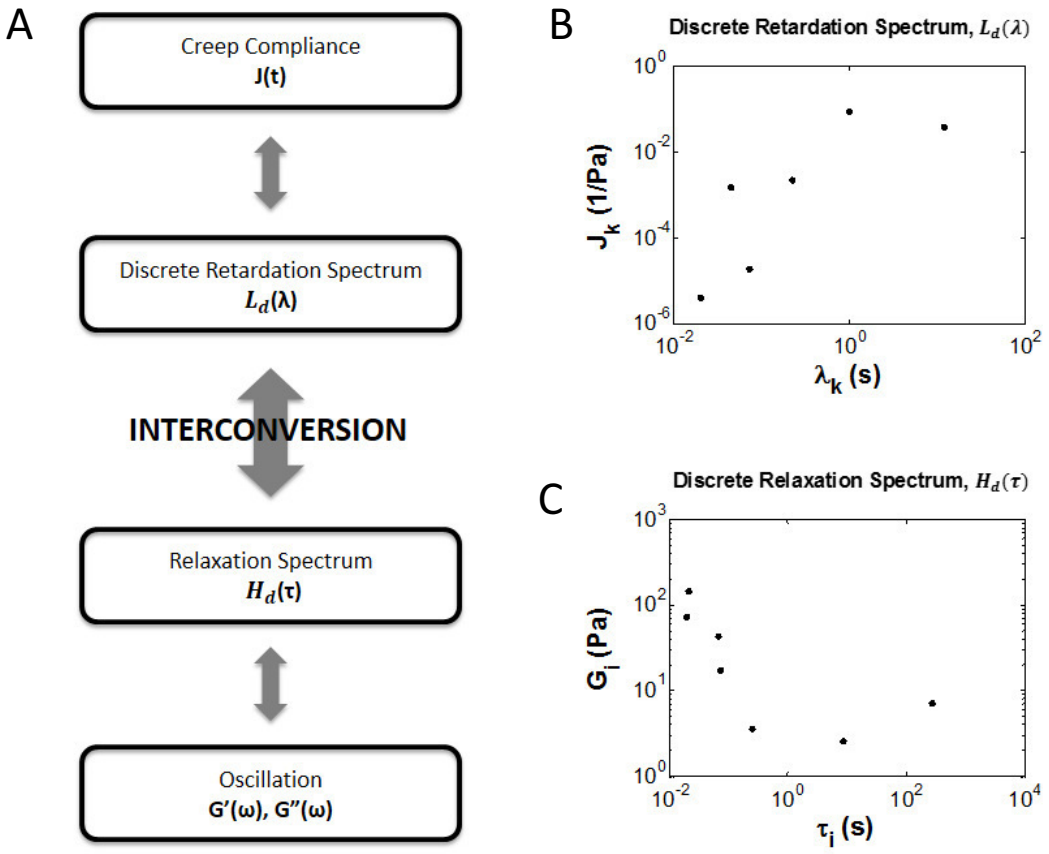

Figure 3: (A) Schematic illustrating the step-by-step interconversion process and the resulting representative (B) discrete retardation and (C) discrete relaxation spectra from the interconversion of infant ovine vitreous.

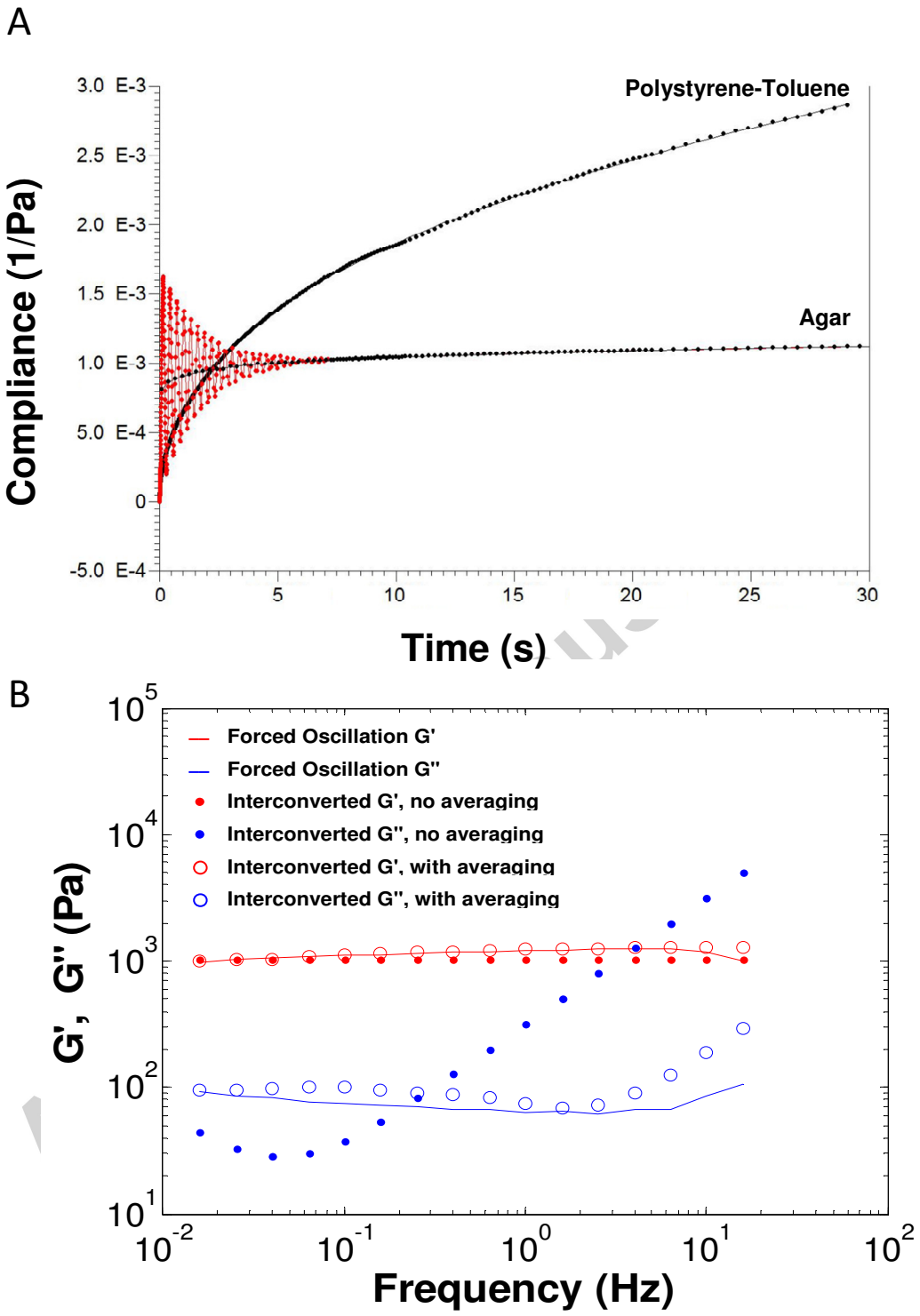

Figure 4: (A) Representative creep compliance curve (■) and retardation fit (-) for polystyrene-toluene and agar. Averaging the creep-ringing region for agar (○) resulted in a damped compliance curve and better curve fit to the material function (Equation 1). (B) The improved curve fit of agar from the averaged data resulted in a better approximation of the dynamic moduli from forced oscillation compared to interconverted dynamic moduli calculated from creep data without averaging.

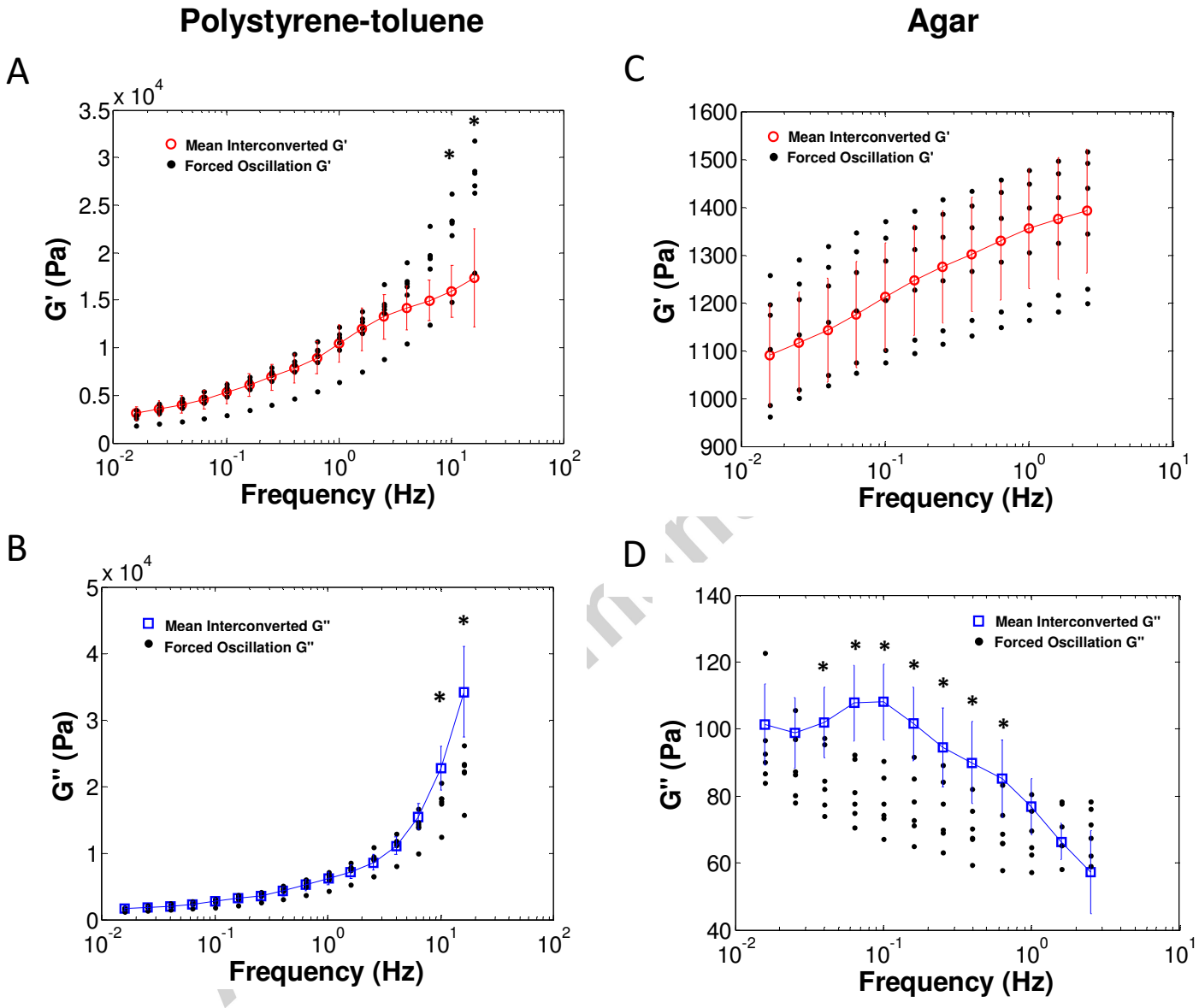

Figure 5: (A) The interconverted G' polystyrene-toluene data was not statistically different from the oscillation G' data up to 10 Hz (*p<0.05). (B) The interconverted G" polystyrene data also became significantly different from the oscillation G" data around 10 Hz (*p<0.05). (C) The interconverted G' agar data was not statistically different from G' measured from forced oscillation at any frequency. (D) The interconverted G″ agar data was statistically different from forced oscillation for 7 of the 12 frequencies in the interconverted frequency spectrum (*p<0.05).

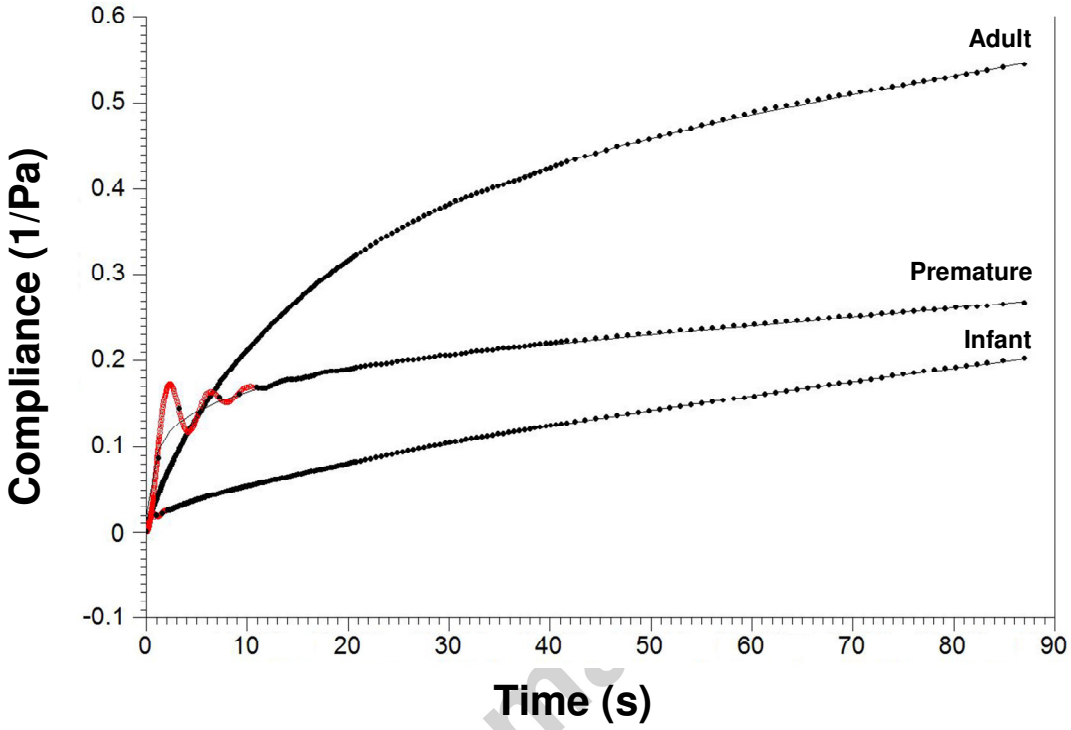

Figure 6: Representative creep compliance curves for premature, infant, and adult vitreous. Averaging the creep-ringing region in the premature and infant (○) resulted in damped compliance curves (■) and better retardation curve fits for each age (-).

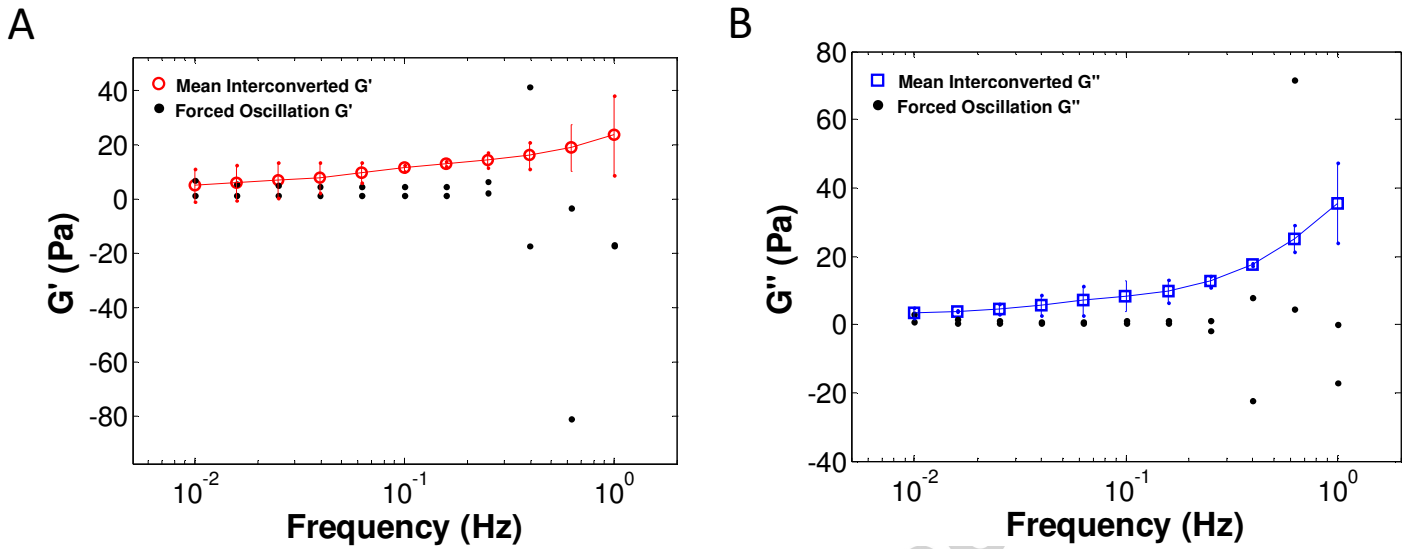

Figure 7: (A) The mean interconverted G' and (B) mean interconverted G" of infant sheep vitreous were nearly identical to that measured from forced oscillation data for the lower frequencies. As frequency increased, tissue degradation occurred and the forced oscillation moduli decreased. At 0.3 Hz, tool inertia and slipping resulted in an unstable response from the forced oscillation tests and the data became unreliable. The interconversion technique was able to extend the reliable data range to 1 Hz.

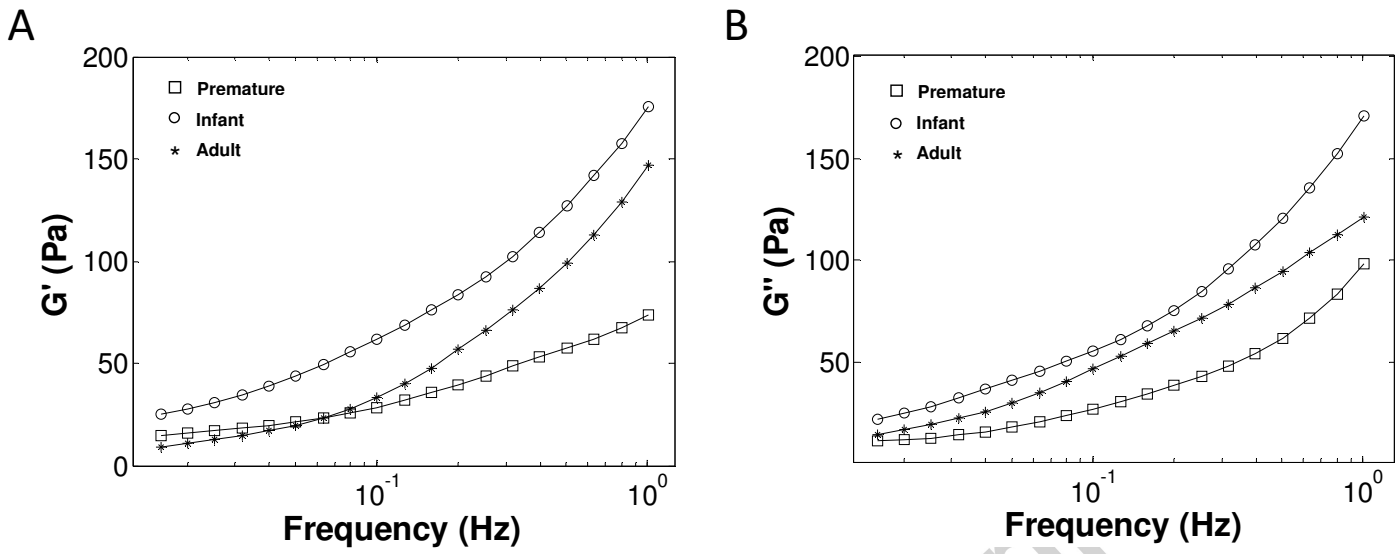

Figure 8: (A) Averaged interconverted G' for each age. (B) Averaged interconverted G" for each age. Large standard deviations were present particularly at high frequencies, and were likely caused by vitreous handling, animal variation and the rapid degradation of the specimens. This resulted in no statistically significant differences despite obvious trends with age. For visual clarity, error bars are not shown.

- Vitreous degrades within minutes *ex vivo*.
- Spectrum interconversion allowed high frequency data from first msec of testing.
- Pediatric vitreous had higher dynamic moduli than adult vitreous.
- Premature vitreous had lower dynamic moduli than both adult and infant.
- Age-related findings correlate with integrity of collagen/hyaluronan in vitreous.